International Journal of Nanomedicine

Dovepress

open access to scientific and medical research

Open Access Full Text Article

ORIGINAL RESEARCH

Carbon Dots-Based Nanozyme for Drug-Resistant Lung Cancer Therapy by Encapsulated Doxorubicin/siRNA Cocktail

Hailing Yu[1,*], Kexin Tang[1,*], Zeyu Cai[2,*], Xi Lin[1], Yongquan Huang[3], Ting Yu[1], Qianqian Zhang[1], Qiang Wang[4], Lili Wu[5], Lei Yang[6], Hong Shan[1], Hui Luo[1]

[1]Guangdong Provincial Key Laboratory of Biomedical Imaging and Guangdong Provincial Engineering Research Center of Molecular Imaging, The Fifth Affiliated Hospital, Sun Yat-Sen University, Zhuhai, Guangdong, People's Republic of China; [2]Department of Radiology, The Fifth Affiliated Hospital, Sun Yat-sen University, Zhuhai, Guangdong, People's Republic of China; [3]Department of Ultrasound, The Fifth Affiliated Hospital, Sun Yat-sen University, Zhuhai, Guangdong, People's Republic of China; [4]The Green Aerotechnics Research Institute of Chongqing Jiaotong University, Chongqing, People's Republic of China; [5]Key Laboratory for Photonic and Electronic Bandgap Materials, Ministry of Education, School of Physics and Electronic Engineering, Harbin Normal University, Harbin, Heilongjiang, People's Republic of China; [6]Center for Composite Materials and Structures, Harbin Institute of Technology, Harbin, Heilongjiang, People's Republic of China

*These authors contributed equally to this work

Correspondence: Hui Luo; Hong Shan, Email luoh53@mail.sysu.edu.cn; shanhong@mail.sysu.edu.cn

Background: Nanomaterials exhibited intrinsic enzyme-like properties due to the unique properties compared with natural enzyme. Carbon dots (CDs) are an important kind of quantum-sized nanomaterials, which have enormous application potential in bio-imaging, drug carrier, and nanosystems. Carbon dots possess intrinsic enzyme-like properties, such as glutathione (GSH) oxidase or peroxidase activities.

Methods: A co-delivery nanosystem that could carry siRNA and doxorubucin (DOX) simultaneously has been studied in this work. The co-delivery based on carbon dots was surface-modified with poly-ethylenimine (PEI) and loaded the siMRP1 with chemotherapeutics on the surface with pH-triggered drug release. The CD-PEI was synthesized by one-step microwave assisted method; the PEI was raw materials and passivator during the reaction process that makes CDs exhibit excellent optical property.

Results: The CD-PEI was capable of loading and delivering siMRP1 and DOX to tumors and releasing them synchronously in cells in an acid-triggered manner. The particles exhibited GSH oxidase-like catalytic property, oxidizing GSH to oxidized glutathione with concomitant increase of reactive oxygen species (ROS). We found that silencing of MRP1 by co-delivery system antagonized chemoresistance by increasing DOX accumulation and significantly enhancing the inhibitory effect of cell viability induced by CD-PEI-DOX. The co-delivery system dramatically inhibited tumor growth in xenograft model, and CDs counteracted MRP1 function by siRNA-mediated knockdown of MRP1.

Conclusion: Taken together, we uncover the potential role of CDs with a combination of siRNA and chemotherapeutics in overcoming chemoresistance of lung cancer by suppressing MRP1 and oxidation of GSH. Our findings imply its potential of antagonizing chemoresistance to enhance therapeutic efficiency of doxorubicin in clinical practices of lung cancer treatment.

Keywords: carbon dots, chemoresistance, co-delivery, siRNA

Introduction

Nanozymes have attracted increasing attention in the field of enzyme-based diagnosis and cancer therapy, owing to the high catalytic efficiency, high stability and low toxicity. Fe_3O_4, Au, Pt, and graphene are common optimized alternatives for natural enzymes, due to mimic enzyme activities.[1–3] Carbon dots (CDs) are a novel kind of the quantum-sized nanomaterials, which have enormous application potential in bio-imaging, drug carrier, and optoelectronic devices.[4] Carbon dots are composed of carbon atoms, which possess excellent inherent biocompatibility and high catalytic activity.[5] Doping or supported single metal atom is usually the effective method to enhance the catalytic activity of

Received: 17 October 2022
Accepted: 23 January 2023
Published: 21 February 2023

carbon dots, such as peroxidase activity, oxidase-mimetic activity, and catalytic activity.[6] The catalytic activity of carbon dots could disturb oxidative homeostasis of tumor cells. The nanozyme-based catalytic effect of carbon dots is an emerging treatment strategy for tumor therapy, via ROS regulation.[7] Importantly, plenty of reports revealed that CD with surface-modified groups has the capability of delivering multiple drugs simultaneously to the tumor. CD shows negligible cytotoxicity and great chemotherapy efficacy in treating malignant tumors.[8,9]

Lung cancer is the leading cause of mortality among all malignant cancers worldwide.[10,11] Although multiple modalities of therapeutics have been developed including molecular targeted therapy and immunotherapy, chemotherapy remained as a standard option for advanced patients diagnosed with lung cancer.[12,13] However, drug resistance inevitably developed during chemotherapeutic processes, presenting a major impediment in clinical practices.[14,15] Drug concentration in tumor regions was hampered due to devoid of effective delivery methods. Combinational approaches such as integrating anti-neoplastic drugs with novel delivery system would overcome chemoresistance and expand the clinical application of chemotherapeutics.[16] With the advance of nanotechnology, nanomaterials have the advantage to load and selectively release the anti-cancer drugs targeted to the tumor entity, improving treatment efficiency through enhancing drug accumulation.[17] However, even in the context of enough concentration in tumor regions by successful delivery of nanomaterials, therapeutic effect was also restricted by drug accumulation within cancer cells. Drug concentration in cancer cells was greatly affected by the balance between influx and outflux of drugs. Cancer cells utilized several mechanisms pumping drugs out of cells to avoid toxic effect of chemotherapeutics.[18,19] A plethora of proteins were involved in this process including multidrug resistant proteins (MRP1, MRP2, MRP3) and lung resistance-related protein (LRP).[20] However, the mechanisms underlying these molecules are diverse. LRP fulfills its role by redistributing drugs between cytoplasm and nucleus, while MRP family proteins are involved in chemoresistance by enhancing efflux of drugs out of cells to weaken toxic effect of drugs.[21] Modulating signaling molecules involved in these processes would help us to circumvent chemoresistance.

Strategy of co-delivering chemotherapeutics and siRNA targeting chemoresistance-related machinery has been proposed and studied widely in treating malignant cancers such as colorectal cancer.[22,23] Polymer nanoparticles[24] and inorganic nanoparticles[25] have been used as nanoplatform for co-delivering siRNA and drugs. They discovered that co-delivery strategy not only enhances drug delivery through penetration into tumor tissues but also antagonizes chemoresistance by modulating chemoresistance-associated genes.[26] In our previous study, we discovered that the nanocarrier based on carbon dots treatment induced remarkable delivery drugs of doxorubicin to hepatocellular carcinoma tumors.[27] These results led us to further investigate whether CD-PEI nanodrug system could deliver chemotherapeutics and siRNA, realizing both tumor killing and chemoresistance modulation.

In this study, we loaded siRNA targeting MRP1 to antagonize chemoresistance of lung cancer against anti-neoplastic drugs such as doxorubicin based on CD-PEI system (Figure 1). Pivotally, we applied small interfering RNA (siRNA) to down-regulate MRP1 lessening drug efflux and enhancing drug accumulation in lung cancer cells to fulfill the strategy. Carbon dots were fabricated by microwave and surface-modified by polyethyleneimine (PEI). The siRNA and anti-cancer agents were delivered simultaneously to the targeted tumor by CD-PEI. By suppressing drug efflux pumps and modulating oxidative stress, the intercellular uptake of anticancer agents increased and more drugs located at the perinuclear regions. Innovatively, we discovered that our co-delivery system induced suppression of GSH by oxidation and increase of ROS, leading to further suppression of MRP1 function. Our findings would definitely fasten the clinical potential of co-delivery system with a combination of chemotherapeutics and siRNA sequences. Our dual strategy to deliver doxorubicin by CD-PEI and restoring sensitivity by inhibiting MRP1 and simultaneous depletion of GSH would give hints with regard to how to overcome treatment failure in refractory lung cancer patients. These results also help to exploit ROS as an ignitor for inhibiting MRP1 function to fulfill the task of antagonizing doxorubicin chemoresistance in clinical practices by co-delivery strategy.

Materials and Methods

The Synthesis of CD-PEI

CD-PEI was fabricated by the microwave-assisted method with PEI-passivated at the surface.[28] The glycerol and PBS solution (pH 7.4) have been mixed, and PEI (MWCO, 25 kDa) was added to the homogeneous solution. The mixed

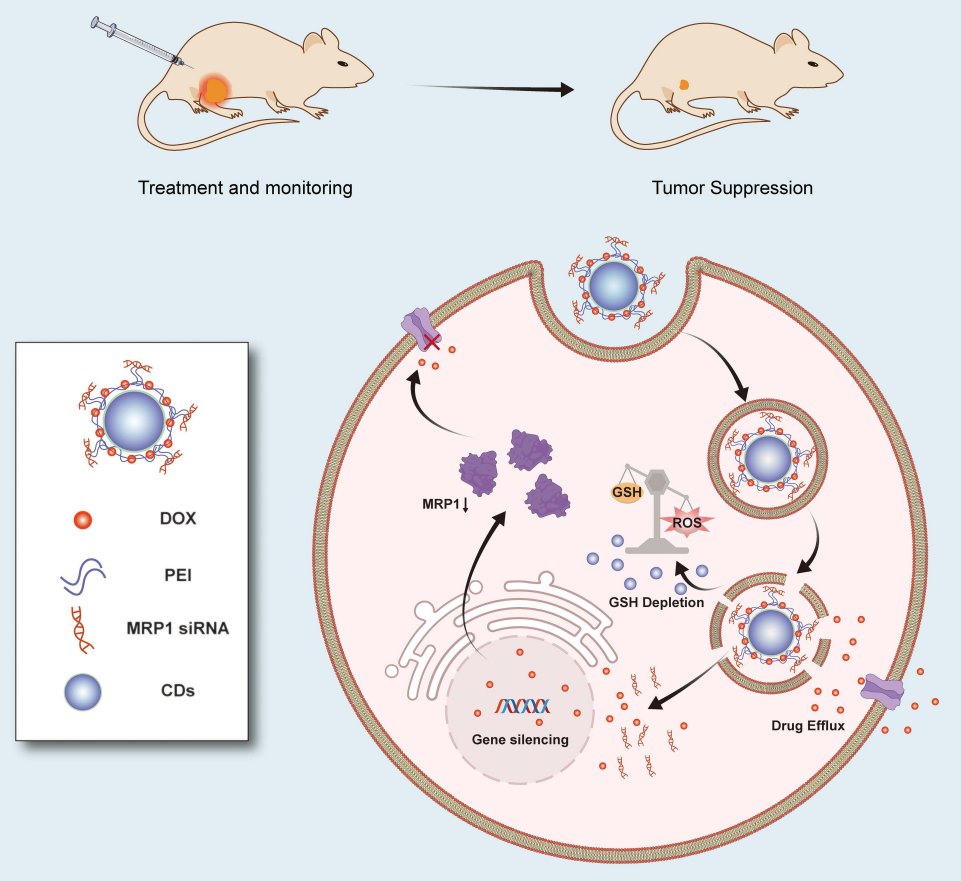

Figure 1 The schematic diagram delineates how CD-PEI-DOX-siMRP1 delivers doxorubicin to tumors and antagonizes chemoresistance by hindering drug efflux through knocking down MRP1 expression.
Notes: Conversion of GSH to GSSG and subsequent ROS increase by CD-PEI oxidase and peroxidase activity further impairs MRP1 function. Collectively, CD-PEI-DOX-siMRP1 was capable of delivering drugs efficiently to tumor entities and retaining them in cells by hindering outflux of MRP1 through synergistic delivery of siRNA and perturbation of GSH -ROS balance.

solution has been transformed into a beaker and placed into a microwave oven for heating 10 minutes. Then, the reaction product was diluted by 10 mL ultrapure water and dialyzed for 2 days to remove the unreacted agents. The solution after dialysis was lyophilized and stored at 4 °C.

The Characterization of CD-PEI and a Nanodrug System Based on CD-PEI

The TEM image of CD-PEI was obtained by high-resolution transmission electron microscopy (JEM-2100), and the X-ray photoelectron spectroscopy of CD-PEI and CD-PEI-DOX were measured by a Thermo 250Xi. The UV-Vis absorbance spectra of the CD-PEI, CD-PEI-DOX, CD-PEI-DOX-siNC, and CD-PEI-DOX-siMRP1 were measured by a Shimadzu UV3600. The PL spectra were characterized by a fluorescence spectrofluorometer (Edinburgh, FLS 980-STM). The Fourier Transform infrared spectroscopy (FTIR) spectra were measured by a Thermo Instruments Nicolet 6700.

Materials and Chemicals

Chemical materials including carbon dots, PEI, and doxorubicin were purchased from Sigma-Aldrich (St. Louis, MO, USA). siRNA targeting MRP1 and negative control sequences were obtained from GenePharma corporation (Shanghai, China). Cell Counting Kit-8 (CCK8) kit was purchased from Dojindo (Kumamoto, Japan). PBS, DMEM medium and fetal bovine serum (FBS) were obtained from Bioscience Biotech Corporation (Shanghai, China). Other chemical reagents were obtained from Kepu Biology Company (Shenzhen, China).

The Loading and Releasing of DOX

The DOX was loaded onto CD-PEI by electrostatic interactions, which has been studied in our previous work.[27] Briefly, the CD-PEI solution mixed with DOX was shaked for 24 h at 4 °C and then dialysed for 3 days to remove the excess DOX agent. The 40 nmol/L MRP1 siRNA was added into the CD-PEI-DOX solution and shaked for 24 h at 4 °C in order to combine them through electrostatic interactions.

The drug loading efficiency of DOX was calculated by the absorbance at 480 nm. The DOX released by CD-PEI-DOX-siMRP1 was measured by the drug release experiment as follows: 2 mL CD-PEI-DOX-siMRP1 solution was added into a dialysis bag (MWCO, 3 kDa) and soaked into PBS solution. After incubation for different intervals, 1 mL PBS solution was gathered and fresh same volume of PBS solution was added. The CD-PEI solution was placed under a 5 W UV flashlight with an excitation wavelength of 365 nm. The drug loading efficiency (DLE) was calculated as follows: DLE% = (amount of DOX in CD-PEI-DOX/amount of DOX) ×100%.[29]

Oxidase-Like and Peroxidase-Like Assays

The oxidation of glutathione (GSH) by CD-PEI was validated by 5.5′-dithiobis (2-nitrobenzoic acid) (DTNB).[30] In a standard Oxidase-like activity assay, 100μg CD-PEI was added into a 1.0 mL buffer solution (pH 4.5) and mixed with aliquots of 10μL of DNTB and different concentrations of GSH. The mixtures were detected in the time interval of 10 min in the absorbance of 422 nm. The peroxidase-like activity was determined by methylene blue (MB) assays, electron spin resonance spectroscopy (ESR), and 2.2′-azino-bis (3-ethylbenzothiazoline-6-sulfonic acid)-diammonium salt (ABTS). Firstly, MB was applied to confirm the peroxidase-like activity. Briefly, a certain quantity of CD-PEI was added into a buffer solution (1.0 mL) containing 10 μL MB (0.416 mM) and H_2O_2 to determine the chromogenic reactions. •OH is detected by electron spin resonance using 5.5-Dimethyl-1-pyrroline-N-oxide (DMPO) as a trapping agent. The ROS is detected using DCFH-DA as an indicator via Incucyte S3 live cell imaging system (Essen Bioscience, Ann Arbor, MI, USA) and confocal laser scanning microscopy (CLSM).

Cell Culture and Cytotoxicity Assays

A549 and A549/ADM cells were purchased from Jennio-bio company (Guangzhou, China). Cells were cultured at 5% CO_2 with atmosphere in a 37°C humidified incubator. The Cell Counting Kit-8 (CCK8) was used to measure the cell viability. Briefly, 1×10^4 of cells were seeded in 96-well plates for 24 hours. The PBS, free DOX, CD-PEI-DOX, and CD-PEI-DOX-siMRP1 were added into the DMEM with different concentrations and incubated for 48 hours. Then, the cells were rinsed and added medium with CCK8 for 1 hour. The absorbance at 450 nm was measured by a spectrophotometer.

Flow Cytometry Assays

Fluorescence-conjugated antibodies were incubated with cells and followed by fluorescence-activated cytometer (Beckman, cytoflex LX Germany). Fluorescence intensity of cells was statistically analyzed and graphed as shown in each figure. For apoptosis assay, cells were incubated with Fluorescein Isothiocyanate (FITC)-labelled Annexin V and propidium iodide (PI) staining buffer, then cells were analyzed by flow cytometry. Annexin V^+ and PI^- cells were considered apoptotic cells.

Western Blot Assays

Western blot assays were carried out following our protocols previously described.[31] Briefly, total cell lysates were prepared in RIPA buffer (Beyotime, Shanghai, China). Total proteins were separated by the sodium dodecyl sulfate-polyacrylamide gel electrophoresis (SDS-PAGE) and transferred to nitrocellulose membranes. After blocking with 5% skim milk for 2 h, the membranes were incubated with the primary antibodies against MRP1 (Cell Signaling Technology, Boston, MA, USA), P-gp (GeneTex, Irvine, CA, USA). Blots then were incubated with the secondary HRP-conjugated antibody (1:5000, Zhongshan Goldenbridge, Beijing, China). Protein bands were visualized using ECL detection reagent and normalized by β-actin (Cell Signaling Technology, Cell Signaling Technology, Boston, MA, USA). Bio-rad

Chemidoc^{TM} XRS^{+} (three Western blots were shown in the supplementary materials. For first blot, exposure time: 0.05 seconds for β-actin, 0.131 seconds for MRP1, 0.321 seconds for p-gP) and Invitrogen iBright system (for second and third blot, exposure time: 0.377 seconds for β-actin exposure time: 1.072 seconds for MRP1) equipments were applied to obtain pictures of chemiluminescence.

Intracellular Drug Release

A549 and A549/ADM cells were seeded and cultured on the Φ15 mm glass battern cell culture dish, respectively. The PBS, free DOX (20 μg/mL), CD-PEI-DOX (DOX concentration, 20 μg/mL), CD-PEI-DOX-siNC (DOX concentration, 20 μg/mL), and CD-PEI-DOX-siMRP1 (DOX concentration, 20 μg/mL) have been added to the culture dish and incubated for 24 hours. After incubation, the cells were rinsed by PBS and observed by laser scanning confocal microscopy (Zeiss LSM 880, Jena, Germany). The cell nucleus is dyed by RedDot^{TM}1. A549/ADM cell mammospheres were seeded in the confocal dish and incubated with nanodrug for the indicated periods.

Animal Study in vivo

All animal studies were conducted in compliance with national guidelines of animal welfare (GB/T 35892–2018) and approved by Animal Ethics Committee of the Fifth Affiliated Hospital of Sun Yat-sen University (Permission No.00145). Briefly, A549/ADM cells were subcutaneously inoculated into 6-weeks old male Balb/c nude mice to construct xenograft models. When tumors grew to palpable size, PBS, DOX and CD-PEI-DOX, CD-PEI-DOX-siNC or CD-PEI-DOX-siMRP1 were injected through tail vein. The bio-distribution of drugs were visualized by in vivo imaging system (IVIS, Perkin Elmer, Waltham, MA, USA) equipment. Hemolysis experiment was performed to assess the biocompatibility of drugs. The targeting of drugs on tumor were visualized and photographed as the indicated time points.

Statistical Analysis

The data between groups were statistically analyzed by Student's *t*-test. $p<0.05$ was used as a criterion for statistical significance.

Results and Discussion

The Characteristic of CD-PEI and Nanodrug System Based on CD-PEI

The TEM images showed that CD-PEI was uniform and spherical, with an average size of 4.25 nm obtained by measuring the sizes of hundreds of CD nanoparticles in TEM images (Figure 2A and B). It is indicated that the average diameter of CD-PEI is 5.503 nm measured by dynamic light scattering (DLS) with the hydration layer (Figure 2C). CD-PEI was dark yellow under white light and well distributed in aqueous solution. Under the ultraviolet light, the CD-PEI solution had obvious green emission indicating that CD-PEI had excellent fluorescence property, as shown in Figure S1. The photoluminescence (PL) spectra of CD-PEI and CD-PEI-DOX-siMRP1 had been characterized by various excitation wavelengths with 20 nm increments as revealed in Figure 2D and E. The emission in carbon dots always results from the nanometer quantum confinement effect.[32,33] The CD-PEI possesses excitation-dependent emission behavior,[34] when the excitation wavelength increases from 330 nm to 510 nm, the emission peak shifts from 450 to 600 nm. The multicolor PL behavior may result from the uneven distribution of emission traps on the surface of carbon dots.[32] In this work, we studied the PL behavior of CD-PEI-DOX-siMRP1 through increasing excitation wavelength from 270 to 510 nm. The PL spectra of CD-PEI and CD-PEI-DOX-siMRP1 were obviously different due to the addition of DOX. The CD-PEI-DOX-siMRP1 had no obvious emission peak when the excitation wavelength is lower than 330 nm. When excitation wavelengths increased from 350 nm to 510 nm, the emission intensity of CD-PEI-DOX-siMRP1 increased and reached a maximum at 470 nm.

There is an obvious absorption band corresponding to the O-H stretching in the FTIR spectrum of CD-PEI and PEI, as shown in Figures 2F and S2A. Nuclear Magnetic Resonance (NMR) spectroscopy analysis indicated that PEI was successfully conjugated with CD as revealed in the characteristic peak of PEI in Figure S2B. The absorption peaks centered at 1096 cm^{-1} and 1655 cm^{-1} correspond to the C-O and C=O stretching, respectively. The absorption bands at 1453 cm^{-1}

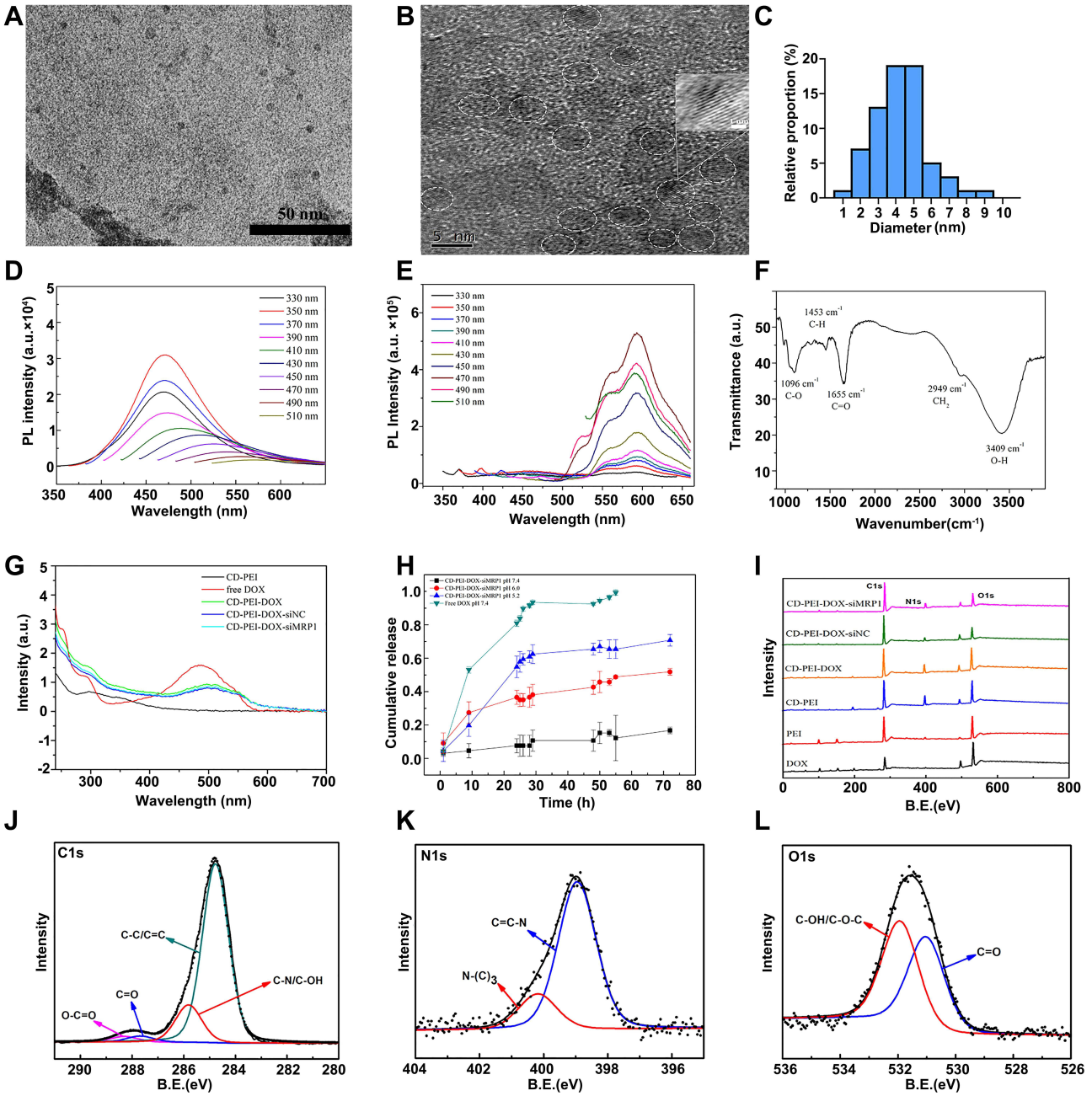

Figure 2 The characteristics of CD-PEI and CD-PEI-DOX-siMRP1.

Notes: (**A** and **B**) The TEM images of CD-PEI (the inset is an auto correlation of the TEM image of the marked area using Digital Micrograph software). (**C**) The diameter distribution of CD-PEI. (**D**) The PL spectrum of CD-PEI. (**E**) The PL spectrum of CD-PEI-DOX-siMRP1. (**F**) The FTIR spectrum of CD-PEI. (**G**) The UV–vis spectrum of CD-PEI, CD-PEI-DOX, CD-PEI-DOX-siNC, and CD-PEI-DOX-siMRP1. (**H**) The release behavior of CD-PEI-DOX-siMRP1 and free DOX under different pH. (**I**) XPS spectrum of PEI, DOX, CD-PEI, CD-PEI-DOX, CD-PEI-DOX-siNC, and CD-PEI-DOX-siMRP1. (**J**) C1s, (**K**) N1s and (**L**) O1s spectra of CD-PEI-DOX-siMRP1.

and 2949 cm^{-1} correspond to the C-H and CH_2 stretching, respectively. The UV–Vis spectrum of CD-PEI in Figure 2G had two bands at 304 nm and 346 nm, corresponding to the π-π* transition and n-π* transition.[35,36] These results confirmed that DOX was loaded on the surface of CD-PEI, and the drug loading efficiency of CD-PEI was 16.7%. The stability of CD-PEI-siMRP1 was investigated by incubating it with various solutions. As shown in Figure S3A and B, no significant precipitation and changes of charges were observed, indicating good serum stability of CD-PEI-DOX-siMRP1 in different

Table 1 Percentage of Groups Obtained from Curve Fitting the C1s and N1s Peaks of Nanodrug

	C1s				N1s		
	C-C/C=C	C-N/C-OH	C=O	O-C=O	C=C-N	N-$(C)_3$	N-H
DOX	66.9%	11.1%	17.1%	4.9%	56.1%	26.5%	17.4%
PEI	79.2%	12.1%	4.5%	4.2%	48.8%	40.0%	11.2%
CD-PEI	65.0%	28.4%	6.6%		69.8%	30.2%	
CD-PEI-DOX	45.5%	33.8%	12.8%	7.9%	65.7%	30.9%	3.4%
CD-PEI-DOX-siNC	63.9%	28.0%	3.3%	4.8%	74.0%	26.0%	
CD-PEI-DOX-siMRP1	78.4%	16.4%	2.7%	2.5%	80.5%	19.5%	

medium. Moreover, the structural stability of CD-PEI-siMRP1 was explored. As shown in Figure S3C and D, no obvious change of size and zeta potential in acid solutions were observed, indicating strong structural stability of our nanoparticle.

The drug release behavior of CD-PEI-DOX-siMRP1 was revealed by in vitro release test (Figure 2H). The free DOX release totally during 50 hours, while CD-PEI-DOX-siMRP1 prolongs the drug release time up to 72 hours when pH was 5.2. CD-PEI-DOX-siMRP1 released minimal DOX under pH 7.4 and illustrated that the nanocarrier would avoid the toxic effect of excessive DOX accumulation in normal tissue and cell. When the pH changed from 7.4 to 5.2, the release amount of DOX from CD-PEI-DOX-siMRP1 increased about 5-times indicating that CD-PEI-DOX-siMRP1 was pH-sensitive and triggered the release of DOX by acid environment.

The information of the chemical composition and functional groups of nanodrug were characterized by X-ray photoelectron spectroscopy (XPS) in Figure 2I. The XPS spectra of CD-PEI-DOX-siMRP1 exhibit three peaks corresponding to C1s peak at 284.5 eV, N1s peak at 399.5 eV, and O1s peak at 531.5 eV, respectively. This result indicates that CD-PEI-DOX-siMRP1 are mainly composed of C, N, and O, with some small inorganic elements due to the synthesis while attaining a solution system at pH 7.4 with PBS.[37] The C1s spectrum of CD-PEI-DOX-siMRP1 (Figure 2J) shows four peaks at 284.8 eV, 285.8 eV, 287.7 eV, and 288.3 eV, which are attributed to C-C/C=C (78.4%), C-N/C-OH (16.4%), C=O (2.7%), and O-C=O (2.5%), respectively. The N1s spectrum of CD-PEI-DOX-siMRP1 (Figure 2K) exhibits two components located at 398.9 eV and 400.2 eV, assigned to C=C-N (80.5%) and N-$(C)_3$ (19.5%) groups. The O1s spectrum of CD-PEI-DOX-siMRP1 (Figure 2L) shows two peaks at 531.0 eV and 531.9 eV, which are corresponded to the C=O (47.7%) and C-OH/C-O-C (52.3%) groups. As shown in Table 1, the change in the chemical groups and the percentage of the nanodrug in the spectra gives further evidence of successful complex conjugation.

Glutathione Oxidase-Like and Peroxidase-Like Nano-Enzyme Activities of CD-PEI

Nanoparticles were widely demonstrated to possess nano-enzyme activities.[38] The result revealed that CD-PEI exhibits excellent GSH oxidase-like nano-enzyme property in a time-dependent manner, as shown in DNTB assays (Figure 3A). Conversion of GSH in oxidized glutathione (GSSG) arouses H_2O_2 and perturbs the oxidation-reduction homeostasis of cells. Thus, we study the peroxidase-like activity of CD-PEI by a series of experiments. Firstly, we used Methylene Blue (MB) to study the property of CD-PEI reacted with H_2O_2 to produce •OH. The results indicated that the CD-PEI possesses catalytic activity to reduce H_2O_2 (Figure 3B), and the ESR assay (Figure 3C) also consistently revealed that CD-PEI is capable of converting H_2O_2 to •OH, which was shown by the characteristic peak trapped by 5.5-dimethyl-1-pyrroline N-oxide (DMPO). As shown in Figure 3D, the absorption spectrum of the oxidized product from the ABTS−H_2O_2 reaction system using the CD-PEI as the peroxidase-like catalyst showed significantly higher absorbance than that of other three reaction systems (CD-PEI+H_2O_2, ABTS+CD-PEI, ABTS+H_2O_2). The results revealed that CD-PEI catalyzed the oxidation of ABTS in the presence of H_2O_2. The depletion of GSH always resulted in the increase of H_2O_2 and •OH, both of which are members of reactive oxygen species (ROS). Thus, we detect the generation of intracellular reactive oxygen species using 2′,7 ′-dichlorodihydrofluorescein diacetate (DCFH-DA) probe. The generation of ROS in cancer cells was detected in laser confocal scanning microscopy and Incucyte system. The results indicated that CD-PEI induces the generation of ROS in cancer cells and the level is concentration-dependent (Figure 3F and G). The generation of ROS is produced within the oxidation process of GSH into GSSG, due to the oxidase-like property of CD-PEI, revealed that the

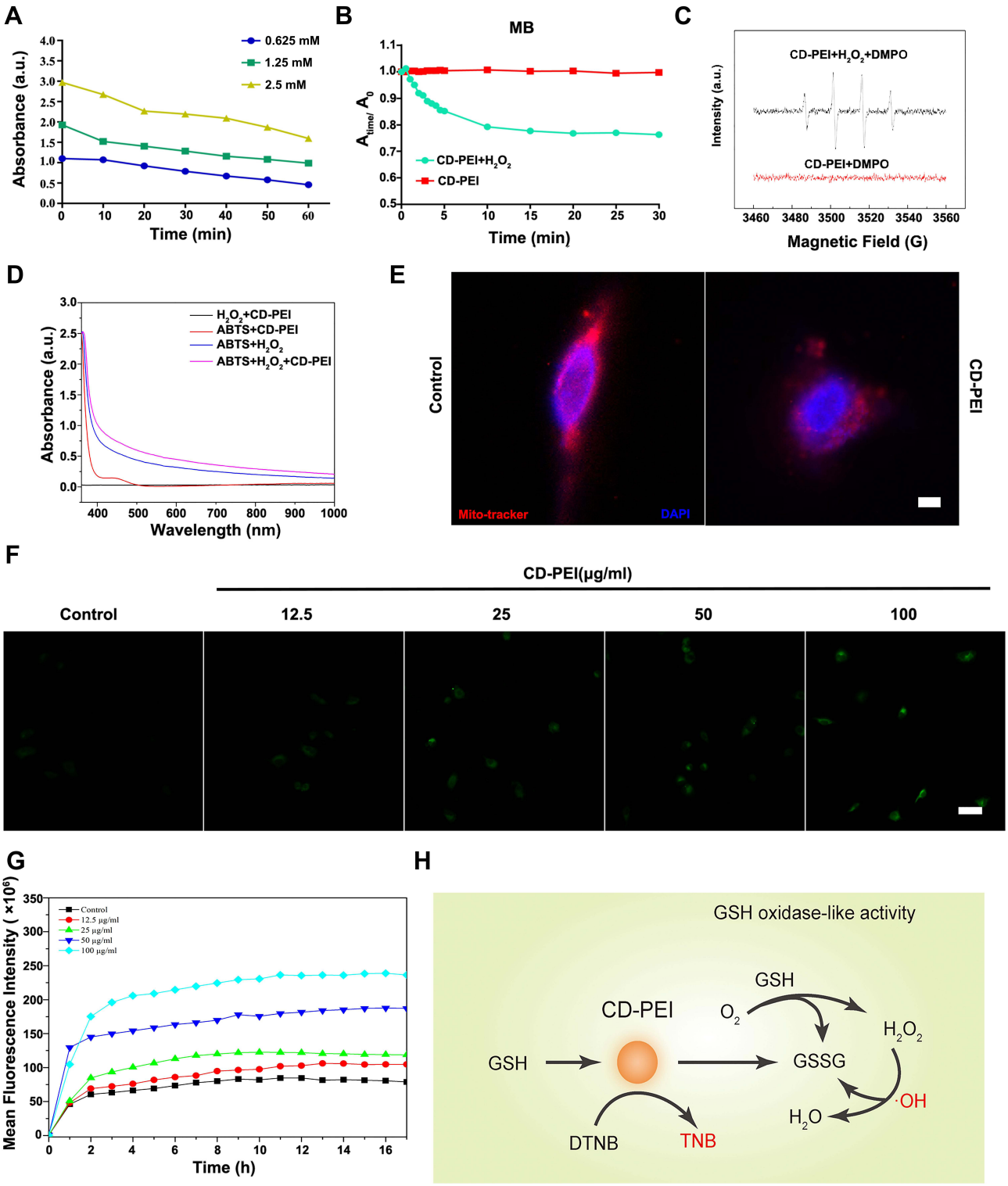

Figure 3 CD-PEI catalyzes the oxidation of GSH and increase of ROS in cells.

Notes: (**A**) The time-dependent behavior of the depletion of GSH in the presence of GSH (0.625 mM, 1.25mM and 2.5 mM) and CD-PEI (200 μg/mL) was analyzed; (**B**) the detection of •OH in the presence of CD-PEI and H_2O_2 using MB probe; (**C**) ESR spectra of •OH trapped by DMPO in the presence of CD-PEI and H_2O_2; (**D**) ABTS–H_2O_2 chromogenic system was used to assess the peroxidase-like activity of CD-PEI. Different solutions were tested as indicated. A full range spectrum absorbance was analyzed and shown. (**E**) The CLSM images of mitochondrial fragmentation in A549 cells (scale bar is 5 μm); (**F**) the CLSM images of ROS generation in A549 cells using DCFH-DA staining, green signals indicate ROS (scale bar is 50 μm). (**G**) The ROS generation in A549 cells using DCFH-DA staining measured by real-time cell monitoring system (Incucyte). (**H**) The schematic diagram indicated the nano-enzyme activity of CD-PEI.

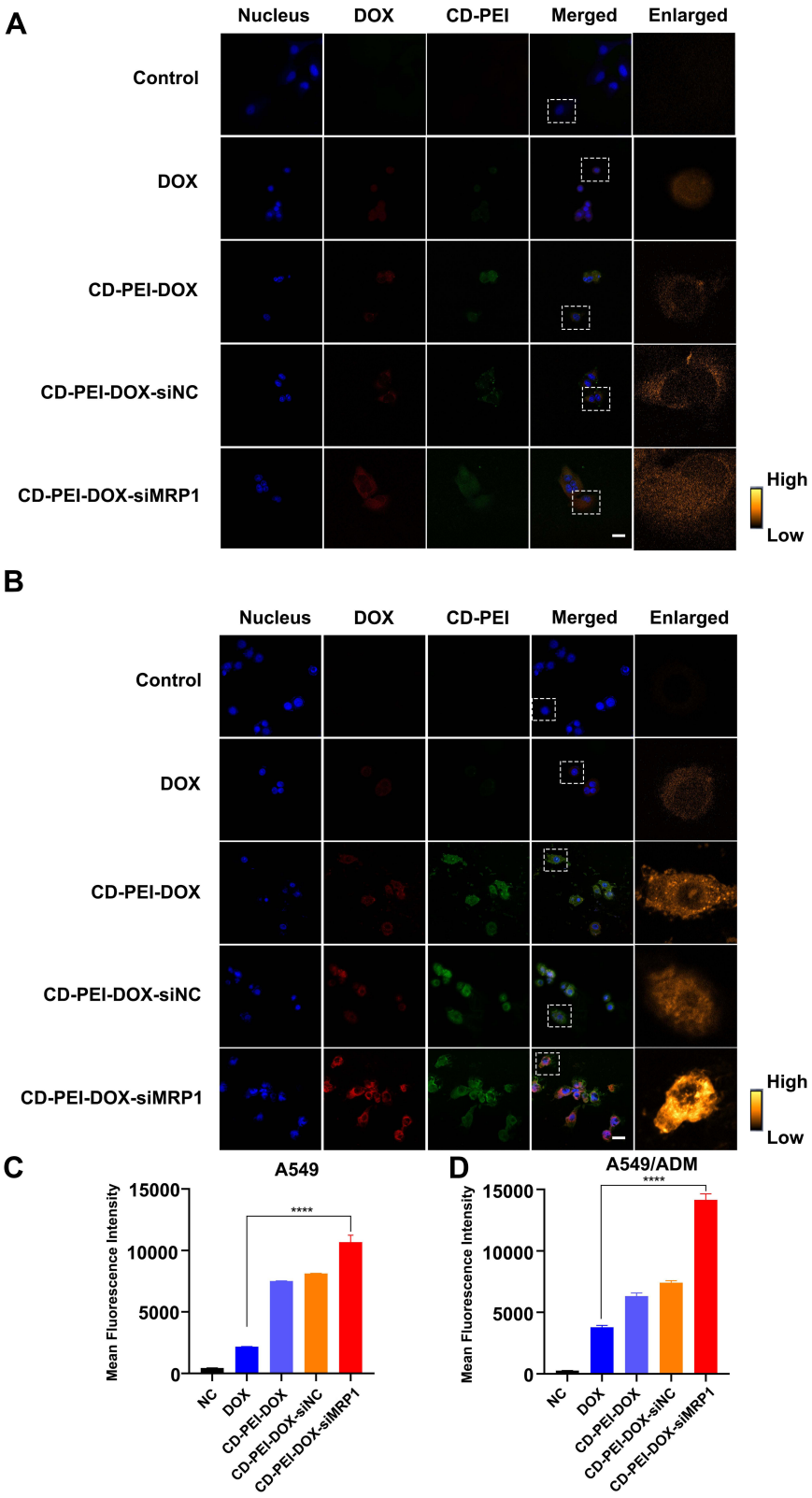

Figure 4 The uptake of cells treated with indicated drugs detected by laser confocal scanning microscopy.

Notes: A549 (**A**) and A549/ADM (**B**) cells were treated with PBS (Control), DOX, CD-PEI-DOX, CD-PEI-DOX-siNC, and CD-PEI-DOX-siMRP1, respectively. Representative pictures were taken under confocal microscopes using 40X oil lens. Blue and red signals indicate nucleus and doxorubicin. CD-PEI was manifested by green signals. Signals were merged using the same field. DOX distribution in white rectangle region of the fourth panel was enlarged and reflected by densometric scale as shown in the fifth panel. (**C** and **D**) The quantitative analysis of the fluorescence intensity of DOX in A549 and A549/ADM cells was carried out by ImageJ. The scale bar is 20μm. ****$p<0.0001$.

CD-PEI has the capability of Fenton-like reaction catalytic activity. Plenty of reports revealed that excessive ROS would cause damage to mitochondria, leading to ROS increase in cells. Therefore, we tentatively examined dysfunction of mitochondria after CD-PEI treatment by Mito-tracker staining. As revealed in Figure 3E, CD-PEI induced a structure of mitochondria from elongated shape into puncta dots, implicating the mitochondrial damage, which might induce ROS increase and apoptosis of cells. Collectively, we conclude that CD-PEI catalyze oxidation of GSH and induce ROS increase by interacting with H_2O_2 resulting from conversion of GSH as illustrated in Figure 3H.

The Internalization and Penetration of DOX Based on CD-PEI Nanodrug System

Uptake of nanodrug system is essential for its drug delivery and therapeutic effect. To analyze the uptake of DOX by our system, the cellular uptake of free DOX, CD-PEI-DOX and CD-PEI-DOX nanoparticles loaded with scramble (NC) or siMRP1 sequences were studied by laser scanning confocal microscopy. The A549 and A549/ADM cells were incubated for various drugs for 24 hours. The results revealed that more CD-PEI-DOX-siMRP1 is internalized by the cancer cells and located in the perinuclear regions and the nuclei in both A549 (Figure 4A and C) and A549/ADM cells (Figure 4B and D). The phenomenon indicated that the CD-PEI-DOX-siMRP1 could enhance the permeability of DOX into the nuclei, which is beneficial to increase the therapeutic efficiency of DOX. Results from flow cytometry assays (Figure 5A and B) also validated the findings that CD-PEI promoted the uptake of DOX and accumulation in cells. All the observations show that the co-delivery system may increase the internalization of drugs into the cells, which facilitates therapeutic effect against chemoresistance elicited by conventional drugs alone.

The depth of bulk tumor entity hindered chemotherapeutic effect of anti-cancer drugs markedly. Enhanced penetration into tumor entities is considered pivotal for its tumor killing effect. Based on this, we attempted to illustrate the permeability of nanodrug system into tumor entity. The penetration of CD-PEI-DOX-siMRP1 into the cancer cell spheres has been investigated using the laser scanning confocal microscopy. The Z-stack mode could be used to observe

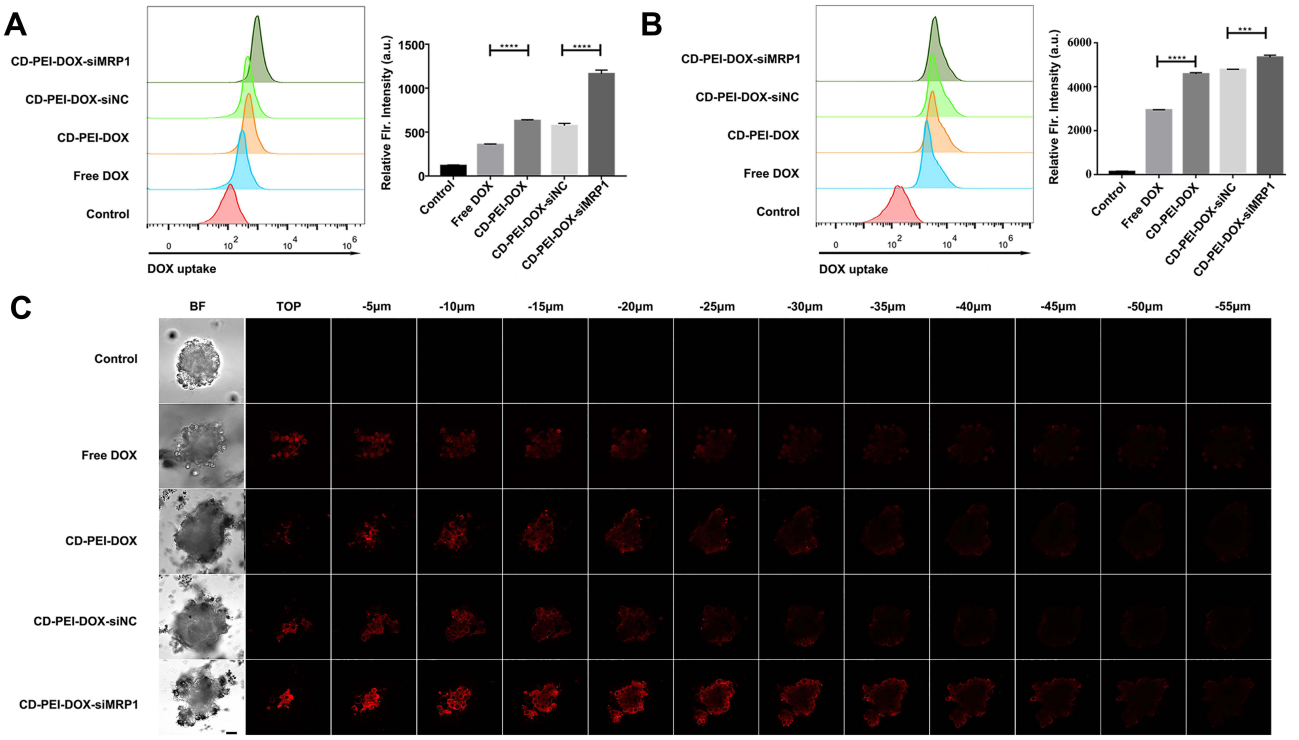

Figure 5 Uptake of drugs in A549 and A549/ADM cells were determined using flow cytometry.

Notes: (**A**) Left panel: A549 cells were treated with the drugs for 8 h, then cells were collected and fluorescence signal of DOX was detected. Right panel: Mean fluorescence intensity of each cell was calculated and statistically analyzed. (**B**) Left panel: A549/ADM cells were treated with the drugs for 8 h, followed by flow cytometry analysis detecting the fluorescence of DOX. Right panel: Statistical analysis of mean fluorescence intensity of DOX in each group. ***p<0.001. ****p<0.0001. (**C**) The penetration of drugs was detected using A549/ADM cells. Confocal Z-stack images of cell mammospheres were obtained and shown after incubated with PBS, free DOX, CD-PEI-DOX, CD-PEI-DOX-siNC, and CD-PEI-DOX-siMRP1. The scale bar is 20 μm.

the penetrate situation of different treatments by gaining the different layers of the cell mammosphere. The results from Figure 5C revealed that the group treated by free DOX has the weakest permeability among all the groups. In addition, the CD-PEI-DOX-siMRP1 could penetrate the inner region of mammosphere. This result confirmed that the CD-PEI-DOX-siMRP1 have the permeability to enter into the inner entity of tumor tissue, which can maximize the therapeutic effect.

CD-PEI-DOX-siMRP1 Inhibits Proliferation and Modulates Chemoresistance by MRP1

Failure of the chemotherapy to malignant tumor was mainly attributable to insensitivity to drugs. Elucidating the mechanisms how tumor cells modulate the chemoresistance was critical for improving the chemotherapeutic effect of various anticancer drugs. We firstly tentatively detected the expression of molecules associated with chemoresistance including p-glycoprotein (P-gp) and MRP1 in adherent, sphere and chemoresistant lung cancer cell line A549. From Figure S4A, we vividly observed that molecules related to chemoresistance were elevated in spheres formed by A549 cells, which were considered to bear more traits of stemness compared with adherent cells. Consistently, these results show that A549/ADM cells expressed a panel of molecules involved in chemoresistance. Subsequently, we analyzed the cell viability of A549 and chemoresistant A549/ADM cells after doxorubicin treatment (Figure S4B). We discovered that A549/ADM cells were resistant to doxorubicin treatment. To further elucidate the role of MRP1 in chemoresistance of lung cancer cells, we attenuate the expression of MRP1 in A549/ADM cells by siRNA-mediated knockdown. To begin with, we determined the most efficient sequence targeting MRP1 in lung cancer cells (Figure S4C–E). Accordingly, siRNA was delivered to cells and MRP1 was successfully silenced by siRNA as revealed by confocal (Figure 6A–D) and flow cytometry assays (Figure S5).

CD-PEI-DOX was conjugated with siMRP1, and CCK8 assays were performed to analyze the cell viability after treatment by various drugs. As shown in Figure 6E and F and Table 2, the IC_{50} of free doxorubicin in A549/ADM cells was approximately 5-fold higher compared with A549 cells. Accordingly, the IC_{50} of CD-PEI-DOX in A549/ADM cells were markedly higher (18.19 μg/mL) than that (6.72 μg/mL) in A549 cells. When CD-PEI-DOX was loaded with MRP1 siRNA sequences, the cells became more vulnerable to CD-PEI-DOX, IC_{50} was only 17.4 μg/mL in A549/ADM cells. Based on these findings, we conclude that the free DOX exhibited different toxic effects to A549 and A549/ADM cells. CD-PEI-DOX-siMRP1 inhibited viability of A549/ADM cells more markedly compared with CD-PEI-DOX groups at all-time points. It implied that siMRP1 enhanced inhibitory effect on cell viability of lung cancer cells elicited by CD-PEI-DOX. CD-PEI-DOX-siMRP1 possesses high toxicity to A549/ADM due to the co-delivery and synergistic effect of siRNA and DOX, indicating that the MRP1 was critically involved in chemoresistance of A549/ADM cells against doxorubicin. To further support the conclusion, Ki67, a proliferation marker, was immunostained and observed under confocal microscopes. The results show that CD-PEI-DOX-siMRP1 inhibited the proliferation of A549 and A549/ADM cells as indicated in Figure 6G–I. Collectively, these results show that MRP1 was involved in chemoresistance of lung cancer against doxorubicin. Moreover, assessment of cell activity was also investigated. As shown in Figure S6, CD-PEI-siMRP1 elicited marked increase of apoptotic A549/ADM cells to 16.86% compared with control. These results indicated that CD-PEI-siMRP1 influence cell viability of chemoresistant lung cancer cells by both inhibiting proliferation and inducing apoptosis.

CD-PEI-DOX-siMRP1 Co-Delivery System Inhibited Tumor Growth in Chemoresistant Lung Cancer Models

To further elucidate the role of MRP1 on chemoresistance of lung cancer, we construct lung cancer xenograft models on nude mice to analyze the targeting and tumor inhibitory effect of our delivery system. As shown in Figure 7A, CD-PEI-DOX shows a specific binding to tumors in our xenograft model even loaded with siMRP1. Intense signals of CD-PEI-DOX-siMRP1 signals were observed to stay at tumor region in a time-dependent manner, while no marked signal was seen in doxorubicin or PBS-treated groups. Furthermore, organs were harvested from mice bearing lung tumors after indicated treatment for 24 hours. As shown in Figure 7B, high retention of doxorubicin in tumors was observed from CD-PEI-DOX-siMRP1 group indicating that silencing MRP1 might realize enhanced accumulation of drugs in tumors. CD-PEI-DOX-siMRP1 exhibited strong signal on tumors compared with DOX group. Besides, tumors from each group were harvested and

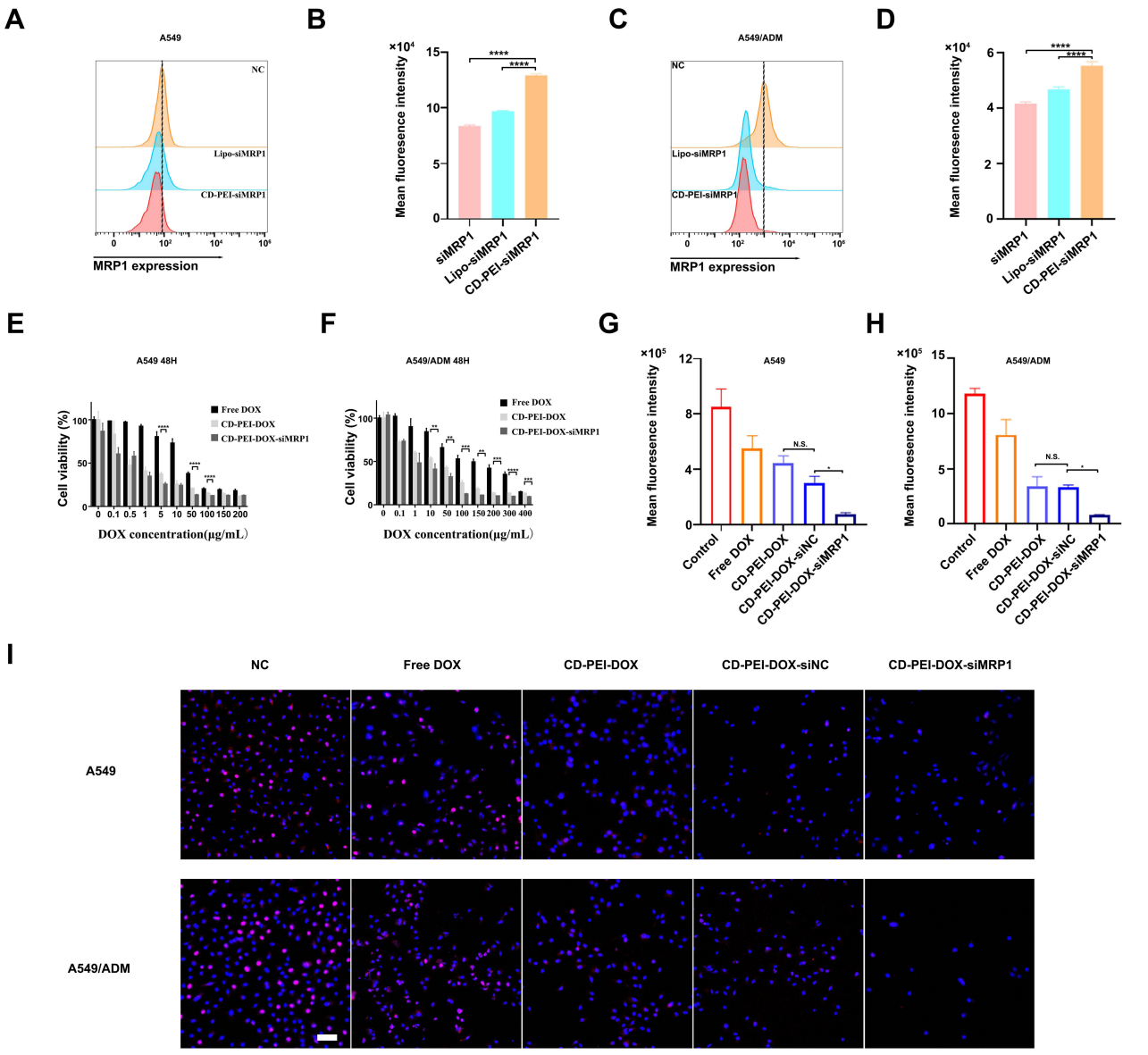

Figure 6 CD-PEI-DOX-siMRP1 inhibits the expression of MRP1 and causes inhibition of proliferation in lung cancer cells.
Notes: (**A** and **B**) Expression and quantification of MRP1 expression on A549 cells by flow cytometry. (**C** and **D**) Expression and quantification of MRP1 on A549/ADM cells by flow cytometry. (**E** and **F**) The cell viability of A549 and A549/ADM cells incubated with free DOX, CD-PEI-DOX, and CD-PEI-DOX-siMRP1 for 48 hours were analyzed by CCK8 assays. (**G–I**) Expression and quantification of Ki67 on A549 and A549/ADM cells by CLSM (Scale bar: 100 μm). *p<0.05, **p<0.01, ***p<0.001. ****p<0.0001.

photographed, which can be seen from Figure 7C. Tumors from CD-PEI-DOX-siMRP1 group were the smallest compared with those of other groups as indicated. Tumor weight and volume were recorded and graphed. The results show that CD-PEI -DOX-siMRP1 inhibited tumor growth markedly evidenced by the tumor weight, volume and inhibition rate (Figure 7D–F).

Table 2 IC_{50} of Free DOX, CD-PEI-DOX, CD-PEI-DOX-siMRP1 in A549 and A549/ADM Cells

IC50 (μg/mL)		
A549	Free DOX	26.993
	CD-PEI-DOX	6.72
	CD-PEI-DOX-siMRP1	5.692
A549/ADM	Free DOX	130.626
	CD-PEI-DOX	18.19
	CD-PEI-DOX-siMRP1	17.4

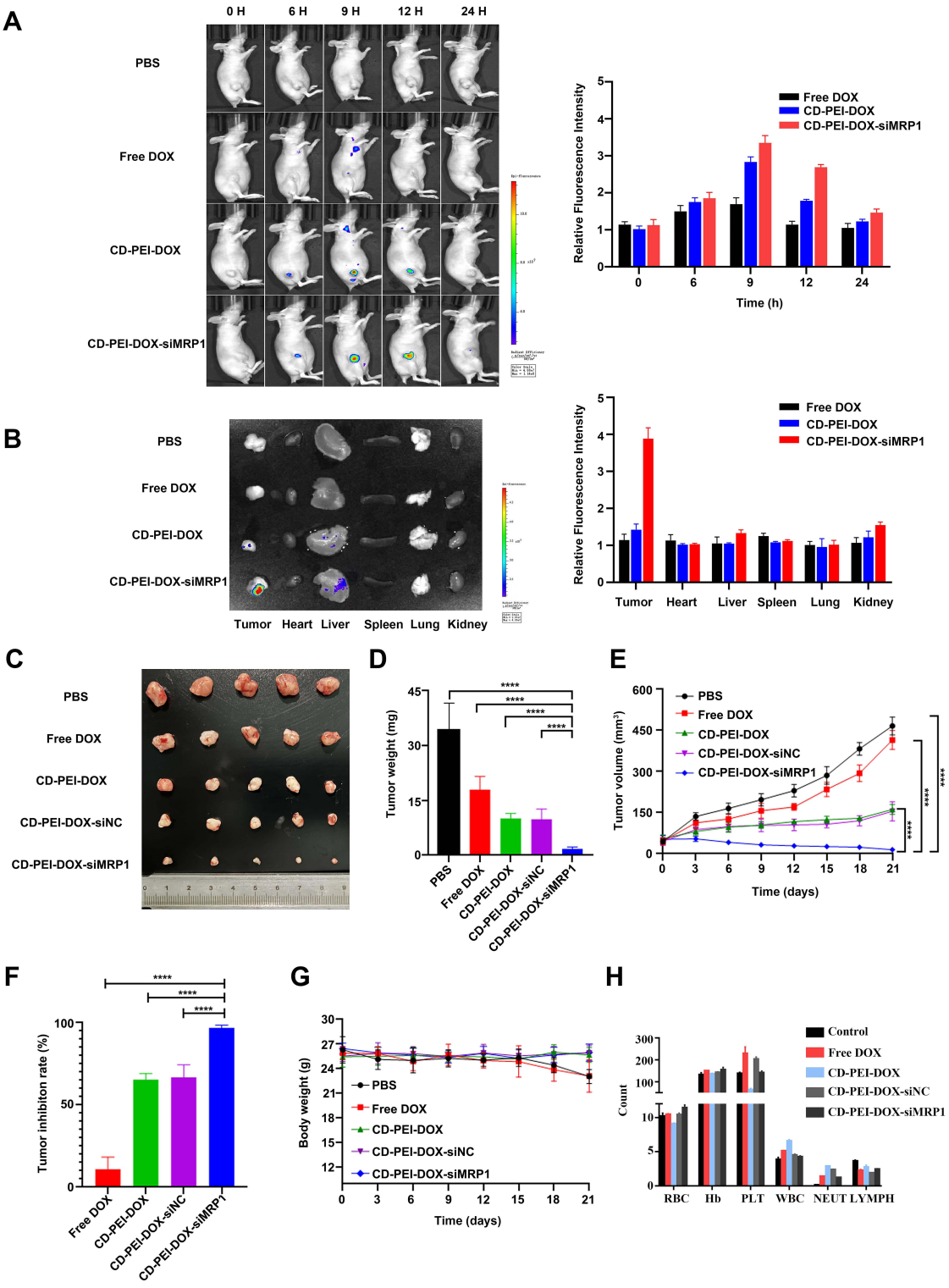

Figure 7 Analysis of targeting and tumor-inhibitory effect of nanodrugs.

Notes: (**A**) PBS, Free DOX and CD-PEI-DOX, CD-PEI-DOX-siMRP1 were injected through tail vein in A549/ADM subcutaneous xenograft model. Left panel: Representative pictures were shown after the indicated treatment for different periods photographed by IVIS. Right panel: Relative immunofluorescence intensity was statistically analyzed from different groups. (**B**) Left panel: Organs of representative group were harvested and photographed under IVIS. Right panel: Relative fluorescence intensity of each organ was calculated and statistically analyzed. (**C**) Tumors were harvested from the mice of each group at the final time point, and representative tumors were aligned and shown (n = 5). (**D**) Tumors from each group were weighed and shown in the graph. (**E**) Tumor volume were recorded and plotted from each group after the indicated treatment. (**F**) Tumor inhibition rate was calculated from each group. PBS-treated group was used as a control. (**G**) Body weight of all mice was recorded and averaged in the indicated group. (**H**) Blood cell analysis was applied to analyze the biocompatibility of indicated drugs. ****p<0.0001.

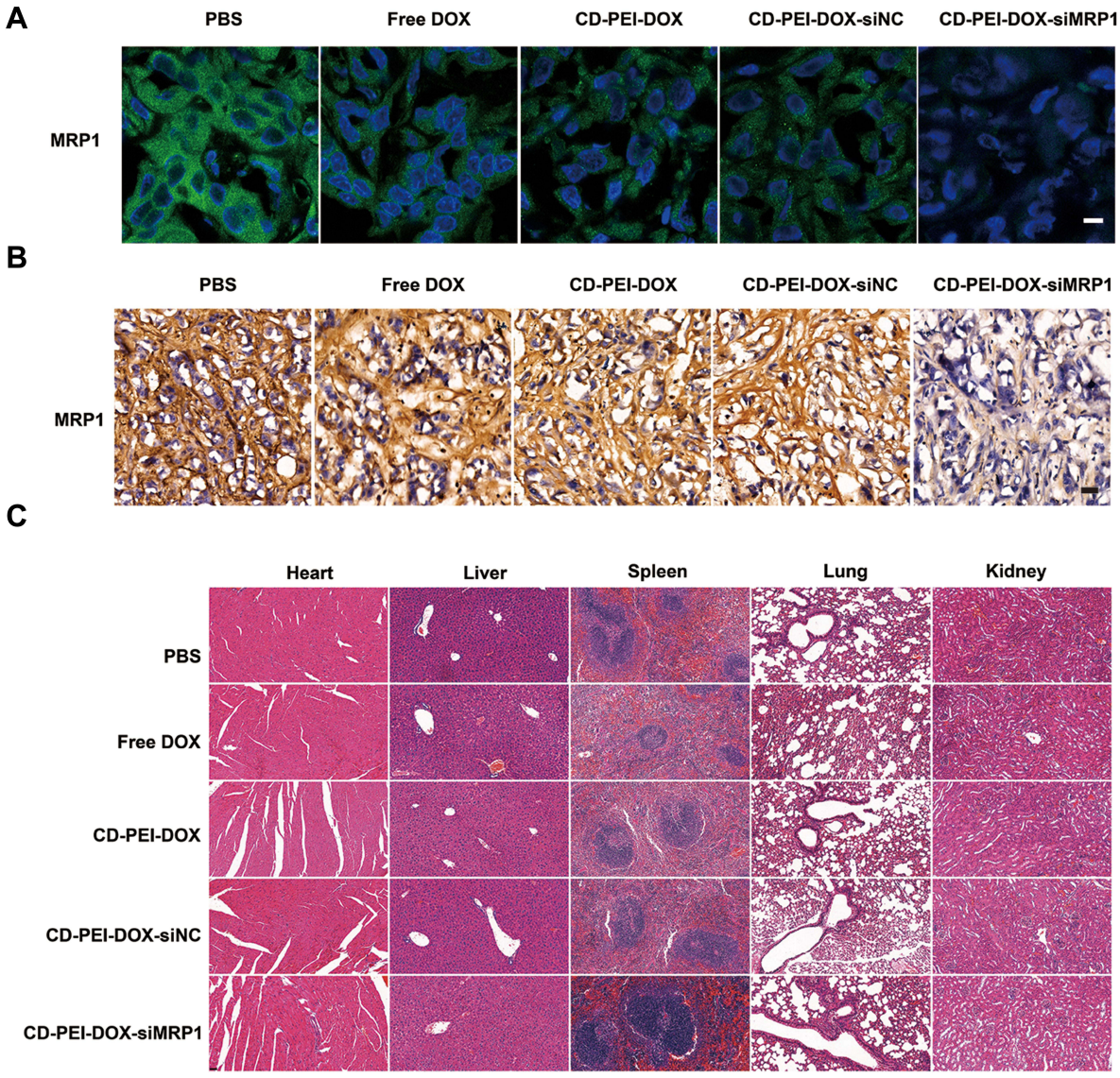

Figure 8 The effect of different drugs on MRP1 expression and tissue integrity on mouse models.
Notes: (**A**) Immunostaining of MRP1 in slices from tumors obtained from each group. MRP1 was visualized with secondary antibody conjugated with Alexa Fluor-488nm fluorescence. Green signal indicates MRP1, while the nucleus was counterstained with DAPI. Scale bar: 25μm. (**B**) MRP1 expression was examined with IHC assays. MRP1 was stained with DAB, and the nucleus was counterstained and shown as blue signals. Representative pictures were shown. Scale bar: 50 μm. (**C**) H&E staining was conducted to determine the toxic effect of various drugs on organs in indicated groups. Scale bar: 50μm.

Importantly, body weights of mice are shown in Figure 7G. Strong biocompatibility of CD-PEI-DOX-siMRP1 could be concluded since no obvious changes were seen in routine blood test as shown in Figure 7H. In consistence with ex vivo results, our co-delivery system are relatively safe and show strong biocompatibility in vivo. These results collectively indicate that knocking down MRP1 could boost the inhibition of tumor growth elicited by CD-PEI-DOX in vivo.

MRP1 Was Involved in Regulation of Chemoresistance Elicited by CD-PEI-DOX Nanodrugs in vivo

To further determine the regulatory effect of our co-delivery system on chemoresistance, we investigate the expression of MRP1 in tumor slices obtained from our xenograft model. Immunostaining experiments show that MRP1 was highly expressed in A549 chemoresistant models as anticipated. The results also indicate that MRP1 was successfully silenced by siMRP1 loaded with CD-PEI-DOX (Figure 8A). Immunohistochemical assays were

performed to investigate the expression of MRP1 in tumor tissues after treatment as indicated. As shown in Figure 8B, MRP1 was highly expressed in normal tissues and CD-PEI-DOX-siMRP1 inhibited expression of MRP1, which is in accordance with immunostaining results. Results from H&E assays (Figure 8C) revealed that no toxic effect is observed after treatment with different drugs, adding a layer of evidence to the conclusion that our nanodrug delivery system has strong biocompatibility in lung cancer models. These results support the conclusion that CD-PEI-DOX is critically involved in antagonizing chemoresistance through modulating MRP1.

Conclusions

In this work, we offered a new approach to overcome the chemoresistance through a strategy of combining siRNA targeted to MRP1 with chemotherapeutic by the co-delivery system based on CD-PEI. The surface of carbon dots was coated with PEI groups, being able to carry siRNA, and the DOX agent was loaded through electrostatic interactions. The co-delivery systems effectively loaded and released siRNA and DOX agents to the targeted tumor, overcoming the resistance to chemotherapy. Conversion of GSH to GSSG and subsequent ROS increase by CD-PEI oxidase and peroxidase activity further impairs MRP1 function. By suppressing MRP1 and depletion of GSH, CD-PEI-DOX-siMRP1 can obviously increase the drug intercellular accumulation and inhibit the proliferation of cancer cells. Results from lung cancer mouse models also revealed that our delivery system inhibits tumor growth without significant toxic effects. These results confirmed that co-delivery systems improve the therapeutic efficiency and overcome the chemoresistance. These works have laid the foundation for exploring the application of anti-cancer drug chemotherapy-resistant delivery systems in the treatment of lung cancer.

Data Sharing Statement

All the data supporting this study are available from the corresponding authors upon reasonable request.

Funding

This work was supported by the Guangdong Basic and Applied Basic Research Foundation (2020A1515011001, 2022A1515012482). It was also funded by grants from the Department of Science and Technology of Guangdong Province to the Guangdong Provincial Key Laboratory of Biomedical Imaging (2018B030322006).

Disclosure

The authors report no conflicts of interest in this work.

References

1. Wu Q, He Z, Wang X, et al. Cascade enzymes within self-assembled hybrid nanogel mimicked neutrophil lysosomes for singlet oxygen elevated cancer therapy. *Nat Commun*. 2019;10:240.
2. Zhong Y, Wang T, Lao Z, et al. Au-Au/IrO2@ Cu (PABA) reactor with tandem enzyme-mimicking catalytic activity for organic dye degradation and antibacterial application. *ACS Appl Mater Interfaces*. 2021;13:21680–21692. doi:10.1021/acsami.1c00126
3. Henna TK, Pramod K. Graphene quantum dots redefine nanobiomedicine. *Mater Sci Eng*. 2020;110:110651.
4. Wareing TC, Gentile AN, Phan ANP. Biomass-based carbon dots: current development and future perspectives. *ACS Nano*. 2021;15:15471–15501. doi:10.1021/acsnano.1c03886
5. Molaei MJ. Carbon quantum dots and their biomedical and therapeutic applications: a review. *RSC Adv*. 2019;9:6460–6481. doi:10.1039/C8RA08088G
6. Lopez-Cantu DO, González-González RB, Melchor-Martínez EM, et al. Enzyme-mimicking capacities of carbon-dots nanozymes: properties, catalytic mechanism, and applications–A review. *Int J Biol Macromol*. 2022;194:676–687.
7. Wu Y, Wei H, van der Mei HC, de Vries J, Busscher HJ, Ren Y. Inheritance of physico-chemical properties and ROS generation by carbon quantum dots derived from pyrolytically carbonized bacterial sources. *Materials Today Bio*. 2021;12:100151.
8. Cohen EN, Kondiah PPD, Choonara YE, du Toit LC, Pillay V. Carbon dots as nanotherapeutics for biomedical application. *Curr Pharm Des*. 2020;26:2207–2221. doi:10.2174/1381612826666200402102308
9. Du J, Xu N, Fan J, Sun W, Peng X. Carbon dots for in vivo bioimaging and theranostics. *Small*. 2019;15:1805087.
10. Siegel RL, Miller KD, Fuchs HE, Jemal A. Cancer statistics, 2021. *CA Cancer J Clin*. 2021;71:7–33. doi:10.3322/caac.21654
11. Hirsch FR, Scagliotti GV, Mulshine JL, et al. Lung cancer: current therapies and new targeted treatments. *Lancet*. 2017;389:299–311. doi:10.1016/S0140-6736(16)30958-8
12. Bray F, Jemal A, Grey N, Ferlay J, Forman D. Global cancer transitions according to the human development index (2008–2030): a population-based study. *Lancet Oncol*. 2012;13:790–801. doi:10.1016/S1470-2045(12)70211-5

13. Frese KK, Simpson KL, Dive C. Small cell lung cancer enters the era of precision medicine. *Cancer Cell*. 2021;39:297–299. doi:10.1016/j.ccell.2021.02.002
14. Kathawala RJ, Gupta P, Ashby CR, Chen Z-S. The modulation of ABC transporter-mediated multidrug resistance in cancer: a review of the past decade. *Drug Resist Updat*. 2015;18:1–17. doi:10.1016/j.drup.2014.11.002
15. Bar-Zeev M, Livney YD, Assaraf YG. Targeted nanomedicine for cancer therapeutics: towards precision medicine overcoming drug resistance. *Drug Resist Updat*. 2017;31:15–30. doi:10.1016/j.drup.2017.05.002
16. Gottesman MM. Mechanisms of cancer drug resistance. *Annu Rev Med*. 2002;53:615–627. doi:10.1146/annurev.med.53.082901.103929
17. Gencer A, Duraloglu C, Ozbay S, Ciftci TT, Yabanoglu-Ciftci S, Arica B. Recent advances in treatment of lung cancer: nanoparticle-based drug and siRNA delivery systems. *Curr Drug Deliv*. 2021;18:103–120. doi:10.2174/1567201817999200730211718
18. Ramos A, Sadeghi S, Tabatabaeian H. Battling chemoresistance in cancer: root causes and strategies to uproot them. *Int J Mol Sci*. 2021;22:9451. doi:10.3390/ijms22179451
19. Begicevic -R-R, Falasca M. ABC transporters in cancer stem cells: beyond chemoresistance. *Int J Mol Sci*. 2017;18:2362. doi:10.3390/ijms18112362
20. Bai H, Wang C, Qi Y, et al. Major vault protein suppresses lung cancer cell proliferation by inhibiting STAT3 signaling pathway. *BMC Cancer*. 2019;19. doi:10.1186/s12885-019-5665-6
21. Hanssen KM, Haber M, Fletcher JI. Targeting multidrug resistance-associated protein 1 (MRP1)-expressing cancers: beyond pharmacological inhibition. *Drug Resist Updat*. 2021;59:100795.
22. Huang C-Z, Zhou Y, Tong Q-S, et al. Precision medicine-guided co-delivery of ASPN siRNA and oxaliplatin by nanoparticles to overcome chemoresistance of colorectal cancer. *Biomaterials*. 2022;290. doi:10.1016/j.biomaterials.2022.121827
23. Zhou Y, Zhang Q, Wang M, Huang C, Yao X. Effective delivery of siRNA-loaded nanoparticles for overcoming oxaliplatin resistance in colorectal cancer. *Front Oncol*. 2022;12:340.
24. Chen S, Deng J, Zhang L-M. Cationic nanoparticles self-assembled from amphiphilic chitosan derivatives containing poly(amidoamine) dendrons and deoxycholic acid as a vector for co-delivery of doxorubicin and gene. *Carbohydr Polym*. 2021;258:117706. doi:10.1016/j.carbpol.2021.117706
25. Creixell M, Peppas NA. Co-delivery of siRNA and therapeutic agents using nanocarriers to overcome cancer resistance. *Nano Today*. 2012;7:367–379. doi:10.1016/j.nantod.2012.06.013
26. Tieu T, Wojnilowicz M, Huda P, et al. Nanobody-displaying porous silicon nanoparticles for the co-delivery of siRNA and doxorubicin. *Bio Sci*. 2021;9:133–147. doi:10.1039/D0BM01335H
27. Hailing Y, Xiufang L, Lili W, et al. Doxorubicin-loaded fluorescent carbon dots with PEI passivation as a drug delivery system for cancer therapy. *Nanoscale*. 2020;12:17222–17237. doi:10.1039/D0NR01236J
28. Liu C, Zhang P, Zhai X, et al. Nano-carrier for gene delivery and bioimaging based on carbon dots with PEI-passivation enhanced fluorescence. *Biomaterials*. 2012;33:3604–3613. doi:10.1016/j.biomaterials.2012.01.052
29. Bai J, Liu Y, Jiang X. Multifunctional PEG-GO/CuS nanocomposites for near-infrared chemo-photothermal therapy. *Biomaterials*. 2014;35:5805–5813. doi:10.1016/j.biomaterials.2014.04.008
30. Zhang H, Yao S, Zhao C, Zhao W, Li J, Wang J. Feasibility study on facile and one-step colorimetric determination of glutathione by exploiting oxidase-like activity of Fe3O4-MnO2 nanocomposites. *Analytical Sci*. 2021;37:1355–1360. doi:10.2116/analsci.20P353
31. Lv X, Yu H, Zhang Q, et al. SRXN1 stimulates hepatocellular carcinoma tumorigenesis and metastasis through modulating ROS/p65/BTG2 signalling. *J Cell Mol Med*. 2020;24:10714–10729. doi:10.1111/jcmm.15693
32. Sun YP, Zhou B, Lin Y, et al. Quantum-sized carbon dots for bright and colorful photoluminescence. *J Am Chem Soc*. 2006;128:7756–7757. doi:10.1021/ja062677d
33. Baker SN, Baker GA. Luminescent carbon nanodots: emergent nanolights. *Angew Chem Int Edit*. 2010;49:6726–6744. doi:10.1002/anie.200906623
34. Hou J, Yan J, Zhao Q, Li Y, Ding H, Ding L. A novel one-pot route for large-scale preparation of highly photoluminescent carbon quantum dots powders. *Nanoscale*. 2013;5:9558–9561. doi:10.1039/c3nr03444e
35. Edison TNJI, Atchudan R, Sethuraman MG, Shim JJ, Lee YR. Microwave assisted green synthesis of fluorescent N-doped carbon dots: cytotoxicity and bio-imaging applications. *J Photoch Photobio B*. 2016;161:154–161. doi:10.1016/j.jphotobiol.2016.05.017
36. Yu P, Wen XM, Toh YR, Tang J. Temperature-dependent fluorescence in carbon dots. *J Phys Chem C*. 2012;116:25552–25557. doi:10.1021/jp307308z
37. Yuan Y, Guo B, Hao L, et al. Doxorubicin-loaded environmentally friendly carbon dots as a novel drug delivery system for nucleus targeted cancer therapy. *Colloids Surf B Biointerfaces*. 2017;159:349. doi:10.1016/j.colsurfb.2017.07.030
38. Yang L, Wang ZR, Wang J, et al. Doxorubicin conjugated functionalizable carbon dots for nucleus targeted delivery and enhanced therapeutic efficacy. *Nanoscale*. 2016;8:6801–6809. doi:10.1039/C6NR00247A